Investigation of Bessel beam propagation in scattering media with scalar diffraction method

Juanjuan Zheng (郑娟娟)[1], Baoli Yao (姚保利)[1], Yanlong Yang (杨延龙)[1], Ming Lei (雷 铭)[1], Peng Gao (郜 鹏)[1], Runze Li (李润泽)[1], Shaohui Yan (严绍辉)[1], Dan Dan (但 旦)[1], and Tong Ye (叶 彤)[1,2*]

[1]*State Key Laboratory of Transient Optics and Photonics, Xi'an Institute of Optics and Precision Mechanics, Chinese Academy of Sciences, Xi'an 710119, China.*

[2]*Department of Neurobiology, University of Alabama at Birmingham, Birmingham, AL 35294, USA*

[*]*Corresponding author: tongtye@gmail.com*

Received July 1, 2013; accepted September 4, 2013; posted online November 4, 2013

Bessel beam propagation in scattering media is simulated using the angular spectrum method combined with slice-by-slice propagation model. Generating Bessel beams with a spatial light modulator, which provides a means to adjust flexibly the parameters of the Bessel beam, allows us to validate the simulation results experimentally. The study reveals that the self-reconstructing length changes oppositely with the axicon angle (i.e., the larger the axicon angle, the shorter the self-reconstructing length). The radius of the incident beam has little influence on the self-reconstruction of the Bessel beam central lobe.

OCIS codes: 260.1960, 170.3660, 290.7050.
doi: 10.3788/COL201311.112601.

The Bessel beam is a type of non-diffracting beam that has gained increasing attention and has been studied intensively[1−4]. Bouchal *et al.*[5,6] reported that the central lobe of the Bessel beam was capable of reconstructing its initial amplitude profile under free propagation after being disturbed by an obstacle. The dynamic propagation of Bessel beams in a volumetric scattering media was also numerically investigated[7,8], and the self-similarity of the Bessel beam after a certain distance propagation in scattering media was experimentally analyzed[9]. In addition, Katsev *et al*[10] used the theory of radiation transfer to investigate the peculiarities of Bessel beam propagation in scattering absorbing media. Rohrbach[11] used the beam propagation method to investigate the propagation of illumination light in the scattering media. The unique optical properties of Bessel beams also allows for many applications. For example, Bessel beam is used as a light source in line-scanned light-sheet microscopes to increase image quality and penetration depth[7,8].

In the absence of a real Bessel beam that possesses infinite power, a quasi-Bessel beam that has a limited power and a limited travel distance can be generated in the laboratory. Bessel beams can be experimentally generated by passing light through metal axicon mirrors[12], round-tip axicons[13], refractive axicon lenses[14], and fluidic axicon lenses[15]. These methods are simple and cost effective; however, adjusting the parameters of the generated Bessel beams is inconvenient. As an alternative, a spatial light modulator (SLM) can be used to generate Bessel beams with the flexibility of tuning their parameters[16].

In this letter, a Bessel beam is generated with a SLM, and influences of various experimental parameters on the self-reconstruction behavior of the Bessel beam central lobe are investigated by virtue of the flexibility of SLM. In addition, the propagation of the Bessel beam in scattering media using a slice-by-slice model and angular spectrum method (ASM) is investigated. Experimental and theoretical results are then compared.

ASM was combined with slice-by-slice propagation model to simulate Bessel beam propagation in the scattering media. The ASM method simulates beam propagation via expanding a complex wave field into a number of plane waves, following the propagation of each individual plane wave through every optical element and medium in the system, as well as summing up their final complex amplitudes. The scattering medium is modeled as a stack of slices, and each slice is assumed to have a thickness of Δ in the z direction (the light propagation direction), as shown in Fig. 1(a). M represents the number of spherical beads that are randomly distributed only on the first surface of each slice and are treated as individual phase retarders. The total phase contribution can be calculated with the summation of the phases of all beads. For the jth bead in the ith slice with a complex refractive index of $\tilde{n}_{\rm bead}$, the phase contribution is simply calculated according to the thickness distribution $d_{ij}(x, y)=2(R^2-r^2)^{1/2}$ along the z direction (Fig. 1(b)). The sum of the optical paths of all the beads in the same layer, $\sum \delta n d_{ij}(x,y)$, contributes to the phase modulation on the beam that passes through this layer. $j = 1, 2, \cdots, M$ denotes the number of beads in the ith slice, and $\delta n=\tilde{n}_{\rm bead}-n$ denotes the refractive index difference between the beads and the medium. Assuming that these beads are not overlapping, the complex transmittance function of the ith slice can be obtained accordingly

$$\widetilde{T}_i(x,y)=\exp\left[\mathrm{i}k\delta n\sum_j^M d_{ij}(x,y)\right]. \quad (1)$$

The real and imaginary parts of δn reflect the refraction and absorption of the jth bead, respectively. By using Eq. (1), the transmittance distribution (a.u.) and the phase distribution (rad) of slice i are shown in Figs. 1(c) and (d), respectively. The propagation process from slice

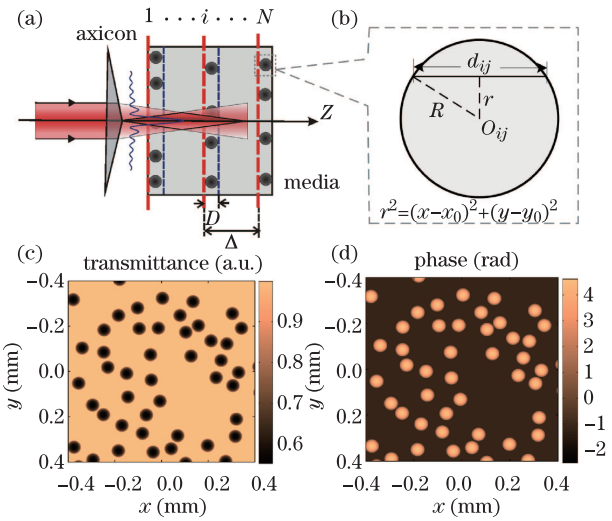

Fig. 1. (Color online) (a) Schematic diagram of Bessel beam propagation in scattering media; (b) the geometry of a spherical bead; (c) the transmittance and (d) phase distributions of the simulated media. (x_0, y_0) denotes the coordinates of the center of the jth bead in the ith slice and (x, y) denotes the spatial coordinates in the x-y plane.

i to slice i+1 can be calculated by using the angular spectrum method[17–19]

$$E_{i+1}(x,y) = \mathrm{FT}^{-1}\{\mathrm{FT}\left(\widetilde{T}_i \cdot E_i(x,y)\right) \cdot \exp\left[\mathrm{i}k_z\Delta\right]\}, \tag{2}$$

where $k_z = k\sqrt{1-(\lambda\xi)^2-(\lambda\eta)^2}$, with ξ and η being the coordinates in the spatial frequency domain. $\mathrm{FT}\{\cdot\}$ and $\mathrm{FT}^{-1}\{\cdot\}$ denote Fourier transform and inverse Fourier transform operators. As the complex amplitude $E_{\mathrm{Bessel}}(x, y, z_{\mathrm{media}})$ of the Bessel beam entering the scattering media is known, the complex amplitude of the beam after any number of slices in the scattering media can be calculated by using Eqs. (1) and (2). This way, the light propagation in the scattering media can be simulated numerically at any given depth of the media.

The presented method is a variation of the scalar wave propagation method[20] and has a similar form as that in the modal propagation method, which is derived directly from the Helmholtz equation[21] and widely used to simulate light propagation in graded-index optical fibers. The presented method calculates the fields propagating from one plane to another by using two fast Fourier transforms. Thus, the computing load is greatly reduced. Another advantage of the presented method is that it can be used for large-angle propagation, where, in general, the Fresnel diffraction method does not perform well[22]. Nevertheless, the presented method is restricted to forward propagation and cannot calculate the back scattering, which is generally investigated by Monte Carlo method[23–25]. Furthermore, the presented method does not take polarization into consideration, so it cannot be used for vector wave propagation, in contrast to that in Ref. [26].

In the simulation, the Gaussian beam with wavelength of λ=632.8 nm has a waist radius of $w_0 = 4.32$ mm. The axicon with open angle $\alpha = 1.11°$ and refractive index 1.51 is located across the Gaussian beam at its waist position to generate the Bessel beam. The refractive index difference between the homogenous media and the beads is $\delta n = 0.05 + 0.005\mathrm{i}$. The diameter of the spherical beads is $D = 60$ μm. The density of the spherical beads in each slice is 20 beads/mm^2. The area of the input beam is sampled with a 1920 × 1080 pixel array with a pixel size of 8× 8 (μm).

Firstly, the propagation process of the Bessel beam in free space is calculated using Eqs. (1) and (2) with $\widetilde{T}_1$=1. The intensity distributions of the Bessel beam in the x–y plane after propagating along the axial direction at the distances of 0, 1, ⋯, and 50 mm, are shown in Fig. 2(a). The non-diffracting property of the Bessel beam central lobe can be clearly seen with its unchanged beam profile after travelling for a long distance of 50 mm. Secondly, the Bessel beam propagation through one layer of scattering is simulated to investigate the self-reconstruction behavior of the Bessel beam central lobe. Some beads are distributed at the plane (denoted with subfigure I in Fig. 2(b)) with a distance of 80 mm from the axicon. The central lobe diameter of the incident Bessel beam is 48 μm, and the diameters of randomly distributed beads are all 60 μm. One of the beads with the aforementioned diameter blocks the Bessel beam central lobe to simulate the self-reconstruction behavior of the Bessel beam central lobe. The complex amplitude distribution of this layer is calculated and denoted with $\tilde{T}_1(x, y)$. After passing this layer, the complex amplitude distribution of the beam becomes $E_t(x, y)$=$\tilde{T}_1(x, y)$ $E_i(x, y)$. The beam intensity distributions after propagating for distances of 0, 1, 5,. . . , and 50 mm are shown in Fig. 2(b). As several beads are located across the beam, the field is severely disturbed because of the absorption and refraction of the beads. However, the simulation shows that the beam intensity profile recovers gradually while propagating for a distance of 5 mm in the scattering medium. The Bessel beam propagating through a thick scattering media is also investigated. The media is composed of seven layers (with a 10-mm distance between the two neighboring layers) filled with random spherical beads. The corresponding transmittance is schematically shown in Fig. 2(c). The volumetric density of the spherical beads in each slice is 2 beads/mm^3. The zoomed central parts of each subfigure in Fig. 2(c) show the relative position between the Bessel beam central lobe and the spherical beads in Fig. 2(d). The beam intensity distributions after propagating through each layer are shown in Fig. 2(e), respectively. The Bessel beam central lobe can penetrate through a thick scattering media, keeping its profile for a long distance.

The experimental setup of the Bessel beam generation and propagation is shown in Fig. 3. A He-Ne laser with a wavelength of 632.8 nm served as the light source, and the intensity and polarization of the laser output were controlled by a neutral filter (NF) and a polarizer P, respectively. The polarizer P was used to adjust the beam polarization to maximize the efficiency of the SLM for phase modulation. Subsequently, the beam was expanded by a beam expander (BE) and illuminated on SLM (Pluto NIR2, HoloEye Inc., Germany, 1920×1080 elements) after passing through a non-polarizing beam splitter (BS). The 0th-order Bessel beam can be generated by loading an axicon phase on the SLM. After reflected by the SLM, the modulated beam passed through the BS and was

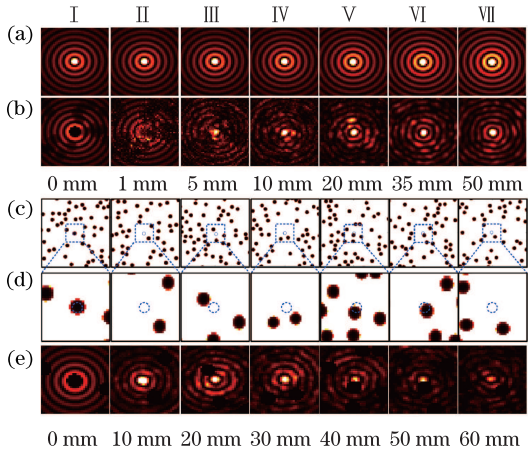

Fig. 2.(Color online) Simulations of the self-reconstruction process of Bessel beam central lobe. (a) The intensity distributions of the Bessel beam after propagating along the axial direction for distances of 0, 1, ⋯, and 50 mm in free space. (b) The intensity distributions in the x-y plane of the Bessel beam propagating for distances of 0, 1, ⋯, 50 mm when blocked by some identical beads. (c) Transmittance distributions of seven layers of scattering beads; (d) zoomed central parts in (c). (e) The intensity distributions of the Bessel beam after passing through each layer of scattering media. The blue dashed circles in (d) denote the positions of the Bessel beam central lobe in each slice.

relayed by a telescope system L_1-L_2 to the sample plane. Considering that the Bessel beam has a ring shape in the spatial frequency plane, an annular aperture was used to filter out some components that did not belong to the Bessel beam. Thus, the quality of the Bessel beam improved noticeably.

In the experiment, a layer of scattering particles (with an average diameter of 60 μm) was stacked on a glass plate and placed across the Bessel beam. The central lobe diameters of the Bessel beam generated with the axicon angles $\alpha = 1.11°$ and $0.68°$ are 48 and 80 μm, which agree basically with the theoretical values of 49 and 80 μm[27]. A CCD camera (DFK 31BU03, Imaging Source Inc., Germany) equipped with a modern L_3-L_4 telescopic lens was used to capture images of the sample plane for image recording. By moving the CCD in the z direction, the intensity distribution of the Bessel beam passing through the sample was recorded. The parameters influencing the self-reconstruction of the Bessel beam central lobe were also investigated.

Firstly, the influence of the axicon angle α on the self-reconstruction of the Bessel beam central lobe is observed. When the radius of the incident beam $R_i = 4.32$ mm is fixed, the self-reconstruction behaviors of the Bessel beam central lobe at $\alpha = 1.11°$ and $0.68°$ are shown in the first row of Figs. 4(a) and (b). The experimental results reveal that for the axicon angle $\alpha = 1.11°$, the Bessel beam central lobe regains its initial intensity profile at a distance of 20 mm, whereas for the axicon angle $\alpha = 0.68°$, the Bessel beam center lobe regains its initial intensity profile with a longer distance of 35 mm. Thus, the self-reconstruction behavior of the Bessel beam central lobe with $\alpha = 1.11°$ is superior to that generated with $\alpha = 0.68°$. For comparison, the self-reconstruction property of the Bessel beam central lobe was also theoretically investigated at $\alpha = 1.11°$ and $0.68°$, and the corresponding results are shown in the second row of Figs. 4(a) and (b). Furthermore, dependence of the self-reconstructing length on the axicon angle is measured, and the result is plotted in Fig. 4(c). The self-reconstructing length is defined as the value that the intensity of the center lobe recovers, which is 75% of the original value. Clearly, the larger the axicon angle, the shorter the self-reconstructing length and the better the self-reconstruction behavior. Results show that the larger the axicon angle, the larger the Bessel beam central lobe, the larger the angle of the incident beam refracted, and the faster the beam gathers on the axis beyond the blocking spot, as shown in Fig. 4(d). However, specific experiments show a limit for the angle α, which governs the spot size of the generated beam. In a microscopic imaging system, the spot size is fixed and the refracted angle of the beam after the axicon is no larger than NA/M, where NA and M are the numerical aperture and the magnification of the imaging system.

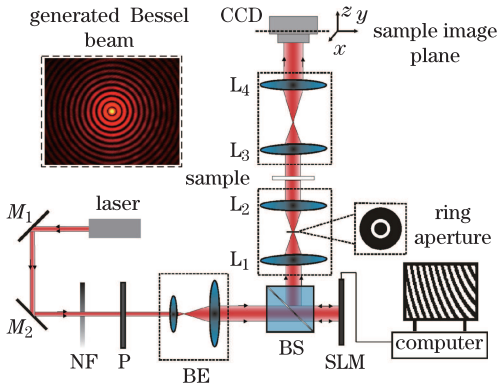

Fig. 3. (Color online). Schematic of the experimental setup for studying Bessel beam generation and propagation. M_1, M_2, mirrors; L_1, L_2, L_3, L_4, lenses with focal lengths: f_1=150 mm, f_2=150 mm, f_3=150 mm, f_4=200 mm, respectively.

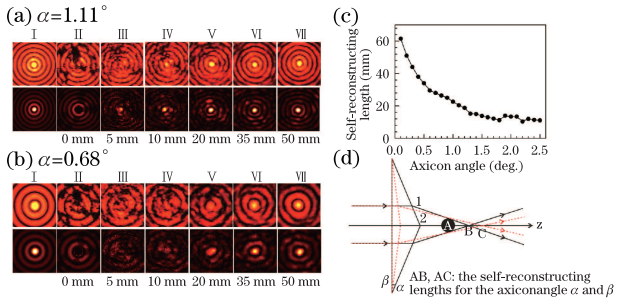

Fig. 4. (Color online). The influence of the axicon angle on the Bessel beam central lobe self-reconstruction. The self-reconstruction of the Bessel beam generated with the axicon angles of (a) 1.11° and (b) 0.68°, respectively. The first and second rows in (a) and (b) show the experimental and simulation results; (c) the self-reconstructing length versus the axicon angle; and (d) geometrical analysis of the influence of the axicon angle. Subfigure I displays the intensity distributions of the Bessel beams right before entering the scattering media; II to VII display the intensity distributions of the Bessel beams at different travel distances in the scattering media.

Secondly, the influence of the radius of the incident beam R_i on the self-reconstruction of the Bessel beam central lobe is investigated. When $\alpha = 1.11°$ fixed, the self-reconstructions of the Bessel beam central lobes under $R_i = 4.32$ and 2.16 mm are illustrated in the first row of Figs. 5(a) and (b). Similarly, the corresponding theoretical simulations are shown in the second row of Figs. 5(a) and (b). The self-reconstructing length versus the radius of the incident beam (R_i=1.1 to 4.3 mm) is plotted in Fig. 5(c). The figure shows that the self-reconstructing length maintains a constant of 20 mm (for a fixed axicon angle α=1.11° and the Bessel beam central lobe diameter is 60 μm). The incident beam radius is much larger than the size of the scattering particle, and the radius of the incident beam has little influence on the self-reconstruction (Fig. 5(d)). When two incident beams with different radii ($R_1 \neq R_2$) pass through the same axicon, the same position point B after blocking and the same self-reconstructing length are retained. The self-reconstructing length of a Bessel beam central lobe is highly related to the diffraction-free propagation range. However, a distinction between the two can be observed: the former is solely determined by the axicon angle but the latter is determined by both the axicon angle and the width of the incident beam. The fixed axicon angle shows that the larger the width of the incident beam, the larger the diffraction-free range. The self-reconstructing length remains constant.

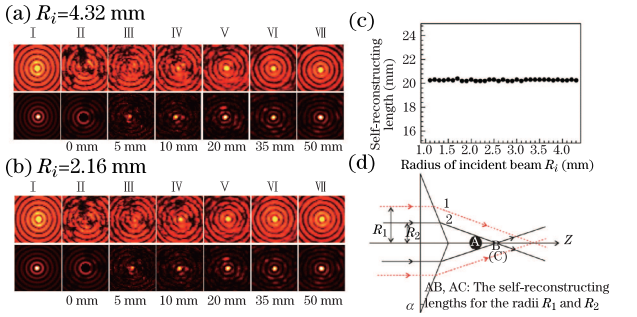

Fig. 5. (Color online). The influence of the incident beam radius R_i on the Bessel beam central lobe self-reconstruction. The self-reconstruction of the Bessel beam central lobe generated with incident radii R_i= (a) 4.32 and (b) 2.16 mm, respectively. The first and second rows in (a) and (b) show the experimental and simulation results; (c) the self-reconstructing length versus the incident beam radius; (d) geometrical analysis for the influence of beam radius.

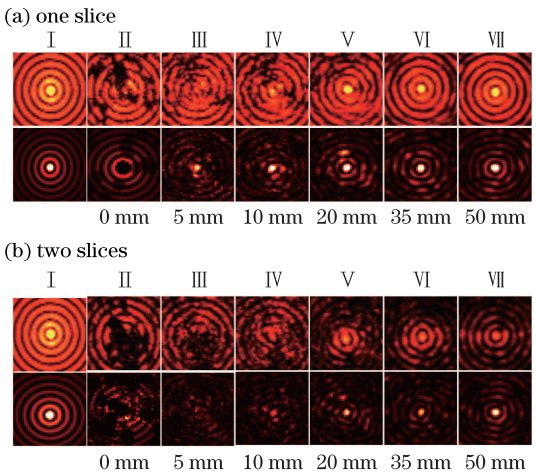

Fig. 6. (Color online). The influence of the number of scattering slices on the Bessel beam central lobe self-reconstruction. Experimental intensity distributions of the Bessel beam passing through (a) one and (b) two slices, respectively (first row), and the corresponding theoretical simulations (second row).

Finally, the thickness of scattering media on the self-reconstruction behavior of Bessel beam central lobe is investigated. In this experiment, the beam propagation is compared between one (one glass plate with scattering particles) and two layers of scattering (two glass plates with scattering particles on their surfaces and placed in parallel distance of 5 mm). The self-reconstruction of the Bessel beam central lobe passing through one and two layers of sample are shown in the first row of Figs. 6(a) and (b), respectively. Results show that the Bessel beam central lobe recovers its shape when passing through either one or two slices of sample, although the intensity of the latter is clearly decreased. The corresponding theoretical simulations are shown in the second row of Figs. 6(a) and (b). Both the simulation and experimental results reveal that the Bessel beam central lobe can retain its characteristics when passing through multiple slices of the scattering media, but exhibits decreased intensity through thicker medium because each slice of scattering medium will cause a certain amount of beam energy to deflect from the original beam. However, other parameters, such as spatial quality of the Bessel beam and size of scattering centers, can also affect the propagation characteristics of a Bessel beam through a scattering media. Considering the theoretical and experimental methods presented, the influence of these parameters can also be investigated.

In conclusion, the propagation of the Bessel beam in scattering media is simulated by using ASM combined with a slice-by-slice propagation model. The theoretical results are verified by experiments using SLM to generate Bessel beams. The simulation and experimental results demonstrate that the axicon angle has distinct influences on self-reconstruction. The larger the axicon angle, the shorter the self-reconstructing length. The radius of the incident beam has little influence on the self-reconstruction of the Bessel beam central lobe. The Bessel beam central lobe can retain its characteristics when passing through multiple slices of scattering media but will lose more energy through thicker media.

This work was supported by the National "973" Program of China (No. 2012CB921900), the National Natural Science Foundation of China (Nos. 61078066 and 61275191), and the Chinese Academy of Sciences under "Hundred-Talents Program" Grant.

References

1. J. Durnin, J. J. Miceli, and J. H. Eberly, Phys. Revs. Lett. **58,** 1499 (1987).
2. J. Durnin, J. J. Miceli, and J. H. Eberly, Opt. Lett. **13,** 79 (1988).
3. F. O. Fahrbach, P. Simon, and A. Rohrbach, Nat. Photon. **4,** 780 (2010).
4. S. Tao and X. Yuan, J. Opt. Soc. Am. A **21,** 1192 (2004).

5. Z. Bouchal, J. Wagner, and M. Chlup, Opt. Commun. **151,** 207 (1998).
6. Z Bouchal, Opt. Commun. **210,** 155 (2002).
7. F. O. Fahrbach and A. Rohrbach, Opt. Express **18,** 24229 (2010).
8. F. O. Fahrbach and A. Rohrbach, Nat. Commun. **3,** 1646 (2012).
9. T. Ersoy, B. Yalizay, and S. Akturk, J. Quantitative Spectroscopy & Radiative Transfer **113,** 2470 (2012).
10. I. L. Katsev, A. S. Prikhach, N. S. Kazak, and M. Kroening, Quantum Electron. **36,** 357 (2006).
11. A. Rohrbach, Opt. Lett. **34,** 3041 (2009).
12. S. K. Tiwari, S. R. Mishra, S. P. Ram, and H. S. Rawat, Appl. Opt. **51,** 3718 (2012).
13. O. Brzobohaty, T. Cizmar, and P. Zemanek, Opt. Express **16,** 12688 (2008).
14. R. Arimoto, C. Saloma, T. Tanaka, and S. Kawata, Appl. Opt. **31,** 6653 (1992).
15. G. Milne, G. D. M. Jeffries, and D. T. Chiu, Appl. Phys. Lett. **92,** 261101 (2008).
16. T. Cizmar and K. Dholakia, Opt. Express **17,** 15558 (2009).
17. J. Zheng, Y. Yang, M. Lei, B. Yao, P. Gao, and T. Ye, Appl. Opt. **51,** 7236 (2012).
18. C. Vecchio and P. Lewin, J. Opt. Soc. Am. **95,** 2399 (1994).
19. P. Gao, B. Yao, I. Harder, J. Min, R. Guo, J. Zheng, and T. Ye, J. Opt. Soc. Am. A **28,** 434 (2011).
20. M. Born and E. Wolf, *Principles of Optics* (Cambridge University Press, Cambridge, 1999).
21. M. D. Feit and J. A. Fleck, Jr., Appl. Opt. **17,** 3390 (1978).
22. K.-H. Brenner and W. Singer, Appl. Opt. **32,** 4984 (1993).
23. E. Alerstam, T. Svensson, and S. Andersson-Engels, J. Biomed. Opt. **13,** 060504 (2008).
24. W. Cai and L. Ma, Chin. Opt. Lett. **10,** 012901 (2012).
25. N. Ren, H. Zhao, S. Zhu, X. Qu, H. Liu, Z. Hu, J. Liang, and J. Tian, Chin. Opt. Lett. **9,** 041701 (2011).
26. M. Fertig and K.-H. Brenner, J. Opt. Soc. Am. A **27,** 709 (2010).
27. P. Dufour, M. Piche, Y. De Koninck, and N. McCarthy, Appl. Opt. **45,** 9246 (2006).